Hindawi
Advances in Civil Engineering
Volume 2019, Article ID 3202959, 19 pages
https://doi.org/10.1155/2019/3202959

Research Article

A Comparative Test Study on the Seismic Damage Sustained by Frame-Core Tube Structures

Zuohua Li, Liang Chen, and Jun Teng

Shenzhen Graduate School, Harbin Institute of Technology, Shenzhen 518055, China

Correspondence should be addressed to Jun Teng; tengj@hit.edu.cn

Received 24 October 2018; Revised 9 January 2019; Accepted 13 February 2019; Published 3 March 2019

Academic Editor: Melina Bosco

The overall damage sustained by a structure can be controlled in the current damage-based seismic design, but the rationality of the relationship among the damage states of the components in the structure and the influences of those states on the overall seismic performance of the structure are currently ignored. In response to this problem, a comparative test was performed in this paper to study the seismic damage performances of two frame-core tube structure models, namely, an optimization model designed through the optimization of the component damage states to achieve the relationship among those damage states proposed in this paper and a normative model designed through the seismic design method based on Chinese codes. By comparing the experimental data of these two models, the relationship among the component damage states was discussed comprehensively, and the influences of those states on the overall seismic performance of the frame-core tube structure were analyzed. The proposed relationship among the component damage states in the optimization model can effectively limit the development of overall damage and improve the internal force response of the structure.

1. Introduction

Damage-based seismic design theory can intuitively control damage behaviors experienced during an earthquake and has consequently received substantial attention spanning a multitude of studies [1, 2]. In early research on damage-based seismic design methods [3, 4], validating calculations of the damage performance replaced those of elastic-plastic deformation, and the damage index did not play a primary controlling role in the seismic design process. In consideration of this problem, various direct damage-based seismic design theories have been proposed [5–7]. Among them, the overall damage can be actively controlled within the seismic design process; however, these theories ignored both the rationality of the relationship among the component damage states throughout the structure and the influences of component damage on the overall seismic performance of the structure. Nevertheless, in the process of damage-based seismic design, the overall damage to the structure must be designed, and the relationship among component damage states throughout the structure must be considered effectively. Thus, the seismic damage performance of the structure, including the rationality of the component damage state relationships and the influences of the damage states of the components on the overall seismic performance of the structure, should be thoroughly understood by the designer to direct the design process.

In the current damage-based seismic design for simple types of structures, such as frame structures and shear wall structures, the design process can be guided by determining the relationship among the component damage states through two seismic concepts, namely, "strong column-weak beam" and "strong wall limb-weak coupling beam" [8–11]. However, in the damage-based seismic design procedure for high-rise building structures, such as frame-core tube structures, the relationships among the component damage states are much more complex than those among the components in simple types of structures due to the diversity of component types. For example, there are relationships among the damage states of the vertical and

horizontal components on the same floor applied to prevent soft-story behaviors; [12] in addition, there are relationships among the damage states of the vertical components on the ground floor and the horizontal components on the upper floors employed to investigate the global damage mechanism [13]; furthermore, there are relationships among the damage states of the vertical components for understanding the cooperative working mechanism of the outer frame and core tube [14]. Accordingly, it is difficult for designers to comprehensively determine and satisfy reasonable variations of the abovementioned relationships among these component damage states in frame-core tube structures through only seismic concepts. Hence, in damage-based seismic design, the influences of the damage states of these components on the overall seismic performance, including the overall structural damage and interstory internal force, should be understood effectively by the designer to actively determine the sensible relationships among the component damage states. To date, it has been proposed that the component damage states will influence the overall structural damage through the damage weighted coefficient; however, this coefficient reflects merely the numerical relationship between the component damage index and the overall damage index, and thus, it cannot reflect the influences of the component damage states on the overall damage of the structure. Although many theoretical analyses and experimental studies on the seismic damage performance have been performed [15–17], the influences of component damage states on the overall seismic performance of frame-core tube structures have not been discussed comprehensively.

Therefore, in this paper, the seismic damage performance of a frame-core tube structure under an earthquake will be studied in detail to direct the damage-based seismic design. To reflect the seismic damage performance of the structure under earthquake activity as much as possible, a series of shaking table tests, which represent one of the most effective tools employed by researchers and designers to understand the seismic performance of structures, was used to comparatively study the seismic damage performances of two scaled models of frame-core tube structures. In these tests, the seismic damage performances of the two models were compared to determine the most reasonable relationship among component damage states therein. In addition, the influences of the component damage states on the overall seismic performance were analyzed, and the interstory internal force was quantified to validate the rationality and advantages of the relationship among the component damage states proposed in this paper.

2. Model Design and Construction

2.1. Model Design. Two models of frame-core tube structures were designed to comprehensively compare their seismic damage performances. One was an optimization model whose component damage states were optimized through finite element analysis, and the other was a normative model designed with the seismic design method based on Chinese codes [18–20]. These two model structures were designed to allow them to reach serious damage states without experiencing overall structural collapse under a rare earthquake, which is in accordance with the target damage states of collapse-forbidden under rare earthquake specified in the Code for Seismic Design of Buildings (GB 50011-2010); thus, the maximum elastic-plastic interstory drift is limited to 1/100 under the rare earthquake to control the target damage states according to the Chinese code.

In the design of the optimization model, the component damage states were optimized to achieve a reasonable damage target that satisfies the damage optimization principles proposed in this paper. Considering that the component damage states can be effectively described based on the concrete material damage states [21], the concrete material damage index in this paper is defined by the degradation of the concrete material unloading stiffness to determine the component damage states according to Chinese codes. The relationship between the material damage index and material unloading stiffness is given as follows: [20].

$$E_d = (1 - d)E_0, \tag{1}$$

where E_0 is the initial stiffness of concrete, E_d is the unloading stiffness of concrete, and d is the tension or compression damage index of the concrete material that can be calculated based on the procedure specified in the Chinese code. For $d = 0$, no damage occurs within the material; for $d = 0.9$, the material fails. Considering that the failure of the concrete component is usually caused by the crushing of the concrete material in the component section, the concrete material pressure damage of the component section is used to determine the component damage. According to the previous literature, the damage index D that represents the average damage value of the components at the same floor is given as follows: [22].

$$D = \frac{\sum_{i=1}^{N} d_n}{N}, \tag{2}$$

where d_n is the maximum concrete material damage value under compression in the component section and N is the statistical number of components at the same floor. To determine the damage of a single component for comparing and optimizing the damage scale of each component in the optimization model, the value of N can be taken as 1; hence, the value of D is equal to the value of d_n. Therefore, the damage index d_n is used to represent the damage of a single component. The component damage index values at different damage levels are given in Table 1 in reference to previous studies [4]. The damage optimization principles and damage scale are summarized as follows:

(1) The horizontal components such as the coupling beam and frame beam in the frame-core tube structure may suffer greater damage considering both their ductility under a nonlinear damage stage and their postyield bearing capacity, which is beneficial for effectively exhibiting a cumulative energy dissipation capacity. Therefore, to permit the

Table 1: Component damage index value at different damage levels.

Damage level	Basic integrity	Slight damage	Moderate damage	Serious damage	Collapse
Damage index	0~0.2	0.2~0.4	0.4~0.6	0.6~0.9	≥0.9

component damage states to reach the corresponding serious damage levels reached under a strong earthquake, the horizontal component damage index is designed to be between 0.6 and 0.9. The cross-sectional reinforcement of the horizontal components can be reduced appropriately to increase the damage index during the damage optimization process.

(2) The damage states of the vertical components such as the frame column and wall limb in the frame-core tube structure should be effectively limited to retain a stable bearing capacity during an earthquake, that is, the damage states of the vertical components (except for the wall limb on the ground floor) should be able to retain their basic integrity under strong earthquake activity; hence, the damage index is controlled within 0.2. In contrast, it is both difficult and unnecessary to retain a state of basic integrity for the wall limb on the ground floor since the wall limb bears most of the base shear and bending moment during an earthquake; hence, the wall limb is permitted to remain in a state of slight damage, and the damage index is controlled within 0.4. The cross-sectional reinforcement of the vertical component may be increased appropriately to decrease the damage index during the damage optimization process.

(3) As they constitute the second design level of fortification under earthquake activity within a frame-core tube structure, the frame columns within the outer frame should possess smaller damage states than the wall limbs in consideration of their collaborative working mechanism.

According to the damage optimization principles, the optimization design steps are as follows:

(1) The optimization model was designed preliminarily according to Chinese codes [18–20] to determine the component section and initial cross-sectional reinforcement.

(2) To ascertain the component damage states, pushover analysis was performed on the structure. To select the lateral load distribution pattern, a modal inertial force distribution pattern was adopted for the pushover analysis according to previous research [23]. A maximum component damage value of 0.9 was established as the target limiting state within the pushover analysis.

(3) Optimize the component damage states. For the horizontal components, reduce the cross-sectional reinforcement if the damage index D_L for the frame beams and the index D_{LL} for the coupling beams are less than 0.6 and end the optimization if the damage indices are greater than 0.6. For the vertical components (except for the wall limb on the ground floor), increase the cross-sectional reinforcement if the damage index D_c for the frame columns and the index D_w for the wall limbs on the upper floors are greater than 0.2 and end the optimization if the damage indices are less than 0.2. However, for the wall limbs on the ground floor, increase the cross-sectional reinforcement if the damage index is greater than 0.4 and end the optimization if the damage index is less than 0.4. The damage relationship between the wall limbs and frame columns should be checked; accordingly, increase the cross-sectional reinforcement of the frame columns if D_c is greater than D_w and end the check if D_c is less than D_w.

(4) Repeat steps 2 and 3 after adjusting the component section reinforcements until the component damage states in the structure satisfy the requirements proposed in the abovementioned damage optimization principles.

(5) Verify whether the maximum elastic-plastic interstory drift satisfies the limiting value specified in the Chinese code [18] under the design earthquake. If the requirement can be met, end the optimization; otherwise, increase the section reinforcements of the vertical components and recheck the interstory drift until it satisfies the limiting value.

The normative model was designed by following the Chinese design code [18–20] to meet the required bearing capacity and deformation. In the design of the component bearing capacity, the seismic forces were evaluated by the vibration mode response spectrum method, and the internal forces of the components were adjusted according to the type of structure, the structural height, and the fortification intensity. The reinforcement for each component was designed by the ultimate limit states design method. To investigate elastic-plastic deformation, the time history analysis method was used to verify the elastic-plastic interstory drift angle under a rare earthquake to avoid overall structural collapse.

To compare the two models, the component section of the optimization model was designed to be the same as that of the normative model, whose prototype component section structure is shown in Table 2. The prototype structures of the two models also have a same total height of 100 m, a constant story height of 4 m, and plan dimensions of 22.8 m × 22.8 m, as shown in Figures 1 and 2. The two prototype buildings are assumed to be located in a region with a seismic design intensity of 7 and a site class of II. The floor loads of the structure are designed according

Table 2: Component section of prototype structure.

Floor	Frame column (mm)	Outer frame beam (mm)	Inner frame beam (mm)	Coupling beam (mm)	Thickness of wall (mm)
1~5	1100 × 1100	400 × 700	400 × 700	400 × 700	400
6~10	1100 × 1100	400 × 800	400 × 800	400 × 800	400
11~15	800 × 800	400 × 900	300 × 900	300 × 900	300
16~25	800 × 800	400 × 700	300 × 700	300 × 700	300

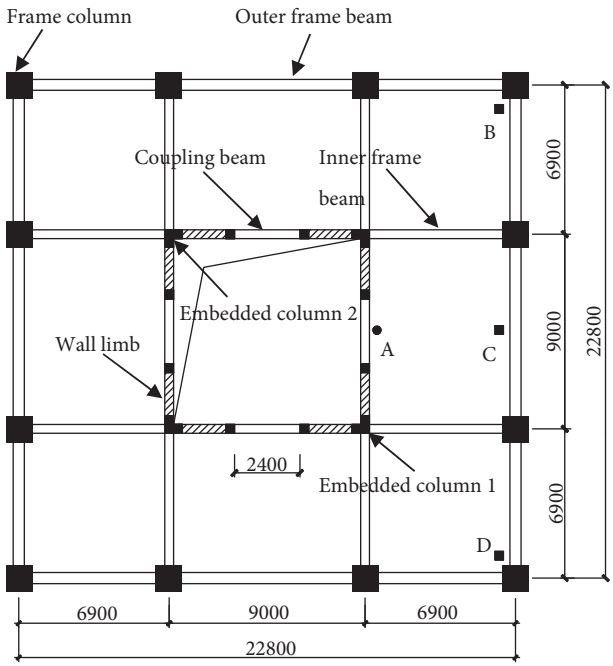

Figure 1: Structure layout.

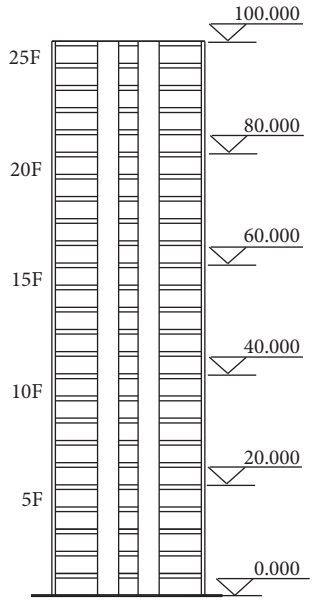

Figure 2: Structure elevation.

to the Load Code for the Design of Building Structures (LCDBS GB 50009-2012). The component damage scales of the two models are obtained (as shown in Table 3) after the two models are designed. The component cross-sectional reinforcement ratio ρ_O of the optimization model and ρ_N of the normative model can be subsequently acquired, and the value of ρ_O/ρ_N is shown in Tables 4–7. In comparison, the section reinforcements of the vertical components in the optimization model were greater than those in the normative model, whereas the section reinforcements of the horizontal components in the optimization model were smaller than those in the normative model, which is in accordance with the damage optimization principles adopted herein.

2.2. Model Material and Similitude Ratio. The model structure was designed and manufactured according to the structure of the corresponding prototype. Given the similarity requirements, the selected materials must have a lower Young's modulus and a higher volume weight than the prototype materials. In addition, the stress-strain relationship of the selected materials should be similar to that of the prototype materials. In view of these considerations, microconcrete was used to simulate the concrete in the model, and galvanized steel wire was used to simulate the reinforcing bars. To guarantee an appropriate model similarity, factors such as the performance parameters of the shaking table, construction conditions, lifting capacity, and laboratory height should be considered. Based on the capacity and size of the shaking table and the ease with which the model can be fabricated, a scaling factor of 1/15 was chosen for the model dimensions. To determine the acceleration scaling ratio, the influence of laboratory environmental noise on the shaking table experiment, the weight of the experimental model, and the bearing capacity of the shaking table must all be taken into account; therefore, the scaling ratio of the acceleration was determined to be 3. Furthermore, according to the measured concrete stress-strain relationship, the scaling factor for the elastic modulus was determined to be 1/3. The scaling factors for other physical quantities can be derived by the corresponding similarity principles, and the typical scaling factors adopted for the model structure are shown in Table 8.

The basic design principles of the reinforcements in the model are as follows: (a) the bearing capacity of the normal section was controlled in accordance with the equivalent bending capacity principle, and (b) the bearing capacity of the oblique section was controlled in accordance with the equivalent shear capacity principle.

2.3. Model Construction. High precision and quality control were required for the construction of the two models due to the size requirements for the fabrication of scale models.

Table 3: Component damage scale of the two models.

Model	Component type				
	Frame column	Wall limb		Coupling beam	Frame beam
		Upper floors	Ground floor		
Optimization model	$D_c < 0.2$	$D_w < 0.15$	$D_w < 0.4$	$0.6 < D_{LL} < 0.9$	$0.6 < D_L < 0.82$
Normative model	$D_c < 0.49$	$D_w < 0.22$	$D_w < 0.55$	$0.43 < D_{LL} < 0.9$	$0.42 < D_L < 0.82$

Table 4: Value of ρ_O/ρ_N in frame column.

Component	Floor	Stirrup	Flexural reinforcement	
			Corner column	Side column
Frame column	1~5F	1	1.5	1.5
	6~10F	1	1.26	1.26
	11~15F	1	1.4	1.4
	16~25F	1	1	1

Table 5: Value of ρ_O/ρ_N in wall limb.

Component	Floor	Distribution reinforcement		Flexural reinforcement	
		Horizontal	Vertical	Embedded column 1	Embedded column 2
Wall limb	1~2F	1.3	1.3	1.2	1.15
	3~14F	1	1	1.15	1.15
	15~25F	1	1	1	1

Table 6: Value of ρ_O/ρ_N in frame beam.

Component	Stirrup	Location	Flexural reinforcement					
			1F	2~5F	6~10F	11~15F	16~21F	22~25F
Frame beam	1	Beam end	0.67	0.58	0.67	0.53	0.67	0.5

Table 7: Value of ρ_O/ρ_N in coupling beam.

Component	Stirrup	Flexural reinforcement				
		1F	2~4F	5~10F	11~15F	16~25F
Coupling beam	1	0.57	0.67	0.67	0.5	0.57

Table 8: Typical scaling factors for converting model response to full-size prototype response.

Category	Variable	Scaling factor	Note
Dimension	Length	1/15	Controlling parameter of dimension
Material	Strain	1.0	Controlling parameter of material
	Elastic modulus	1/3	
	Stress	1/3	
	Density	5/3	
	Mass	4.938×10^{-4}	
Dynamic behavior	Damping	3.313×10^{-3}	Controlling parameter of the test
	Period	0.149	
	Velocity	0.447	
	Acceleration	3	
	Acceleration of gravity	1.0	

Accordingly, foam plastic was selected for the concrete formwork. Prior to constructing the model, foam plastic boards were incised and shaped according to need. After the galvanized steel wires of a component were bundled, microconcrete was poured with an accompanying vibration until the microconcrete became compact. This process was repeated until all the models had been poured. The quality and verticality of each component were checked continuously throughout the entire construction process. The construction process is shown in Figure 3, the completed

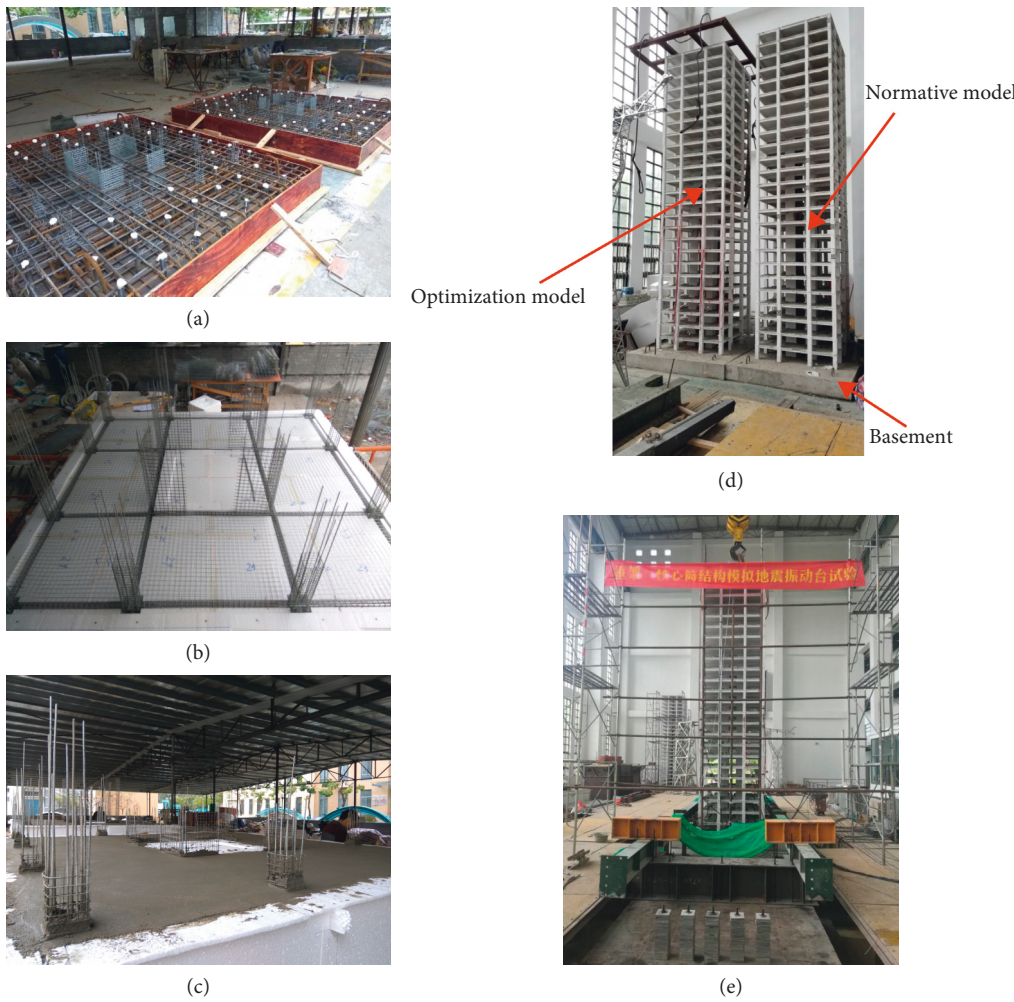

Figure 3: Model construction: (a) basement construction, (b) layout of iron wire and foam template, (c) pouring of microconcrete, (d) finish construction of models, and (e) shaking table model panorama.

model structure is shown in Figure 3(d), and a panorama of the shaking table model is shown in Figure 3(e). After maintenance was performed on the model, the iron blocks of the model counterweights were evenly arranged on the slab. The total height of the model was 6.917 m, of which the basement height was 0.25 m, and the structural height was 6.667 m. The total weight of the model was 13.392 t, of which the basement weight was 4.967 t, and the structural weight was 8.525 t.

3. Test Program

3.1. Instruments and Transducer. To monitor the global responses as well as the local states of the model structures during the experiments, three kinds of sensors were used: an acceleration transducer, a displacement transducer, and an electrical resistance strain gauge. The layout of sensors throughout the model should be arranged effectively according to the force characteristics of the structure. After performing finite element analysis on the damage to the prototype structure, a total of 122 sensors were placed at different measuring points. The acceleration and displacement sensors were arranged evenly along the structural height; the positions of the measuring points on the floors are shown in Figure 1. Seventeen acceleration transducers were installed at measuring point A located in the plan, while sixteen displacement transducers were established at measuring points B, C, and D. To measure the strain and damage of each component in the structure under shaking conditions, strain gauges were placed in unfavorable regions, that is, in regions where the components in the structure are likely to become severely damaged during an earthquake. Through finite element analysis, the regions were determined as follows: (a) the damage region in the frame beam is concentrated mainly at the beam end; (b) the damage region in the coupling beam is concentrated mainly at the beam end and within the oblique section at the midspan of the beam; (c) the damage region in the frame column is concentrated mainly at the column end and the root of the frame column at the base; and (d) the damage region of the wall limb is concentrated mainly at the end of the wall limb. A total of eight-nine strain gauges were installed.

3.2. Input Seismic Waves. The seismic waves are selected according to the Chinese code. The selection principles of frequency contents, intensity, and duration of the seismic waves are as follows:

(1) No fewer than two natural accelerograms and an artificial accelerogram are selected according to the site category and the design seismic group. The average value of the response spectra of the three seismic waves at the primary periodic point of the model structure is no more than 20% of the design response spectrum.

(2) The peak acceleration of each seismic wave should be magnified or reduced to reflect different levels of earthquakes according to the design seismic acceleration peaks specified in the Chinese code.

(3) The duration of each seismic wave should be more than 5–10 times the structural primary period.

According to the abovementioned principles, three earthquake waves, namely, the El Centro wave and the Hollywood wave in addition to an artificial wave, were selected in this paper, as shown in Figure 4. The response spectrum values of the three seismic waves at the primary periodic point were obtained, from which the input sequences of the three earthquake waves were determined as an artificial wave, an El Centro wave, and a Hollywood wave.

3.3. Test Program. The peak accelerations corresponding to different intensities, which were chosen according to the Chinese code (as shown in Table 9), were magnified to obtain the peak accelerations of the seismic input waves for the test cases. The peak acceleration values for the test cases can be magnified to 0.105~0.66 g according to the scaling factor of the acceleration. To further investigate the damage performance under an incredibly rare earthquake, an experiment with an acceleration peak of 0.76 g was performed. Since a comparison of the response spectrum values of the three seismic waves reveals that the response spectrum reaches a maximum under the action of the Hollywood seismic wave, the Hollywood seismic wave was selected for the experiment with an acceleration peak of 0.76 g. A summary of the input waves for these shaking tests is provided in Table 10. During the experiments, a total of 23 working conditions were applied in the normative model and the optimization model. Before the input of each event, white noise was input first to acquire the model dynamic behavior at that moment; simulations of the artificial record, El Centro record, and Hollywood record were then input to the model in succession.

In addition, the durations of the seismic waves should also be reduced according to the scaling factor of the period. The relationship among the periodic similarity ratio, the geometric similarity ratio, and the acceleration similarity ratio can be given as follows:

$$S_T = S_l^{0.5} S_a^{-0.5} = 0.667 \times 1.732 = 0.149, \quad (3)$$

where S_T is the periodic similarity ratio, S_a is the acceleration similarity ratio, and S_l is the geometric similarity ratio. Thus, the time interval and the duration of the seismic waves were reduced to 0.149 times those of the original seismic waves according to the value of S_T, and the input direction was one-way horizontal.

4. Results and Discussion

4.1. Experimental Phenomena. After the tests comprising frequent earthquake intensities of 7 and 8, visible cracks did not appear on the surfaces of the components. The measured natural vibration frequencies of the two models remained constant throughout the tests, thereby explaining why no damage occurred in either model during the experiments. After the test with a basic earthquake intensity of 7, there were still no obvious visible cracks on the surfaces of the components, but the natural vibration frequencies of the two models decreased, indicating that damage had begun to occur in both models. In the tests with a basic earthquake intensity of 7 (0.15 g) and a rare earthquake intensity of 7, the models exhibited slight levels of noise during the vibrations, and visible cracks appeared in the coupling beam and frame beam; moreover, the natural frequencies of the two models further decreased, indicating that the damage in the two models became further aggravated. To evaluate the damage suffered by the components during the earthquake in greater detail, a test with an acceleration peak of 0.76 g was conducted using the Hollywood seismic wave. During this experiment, the vibration amplitudes of the two models were larger than those during the previous tests, and some concrete debris fell from the model exhibiting obvious noise. After the completion of the test, visible cracks were clearly observed in both models with distributions concentrated on the surfaces of the coupling beams and frame beams. By contrast, no obvious visible cracks were observed on the surfaces of the shear walls and frame columns. Typical examples of cracks in the component are shown in Figure 5.

4.2. Dynamic Characteristics. The frequencies of the two models at different phases were obtained through a white noise scan; the variations in the first two frequencies at the end of each instant phase are shown in Tables 11 and 12. With an increase in the earthquake acceleration, the first two frequencies gradually decreased, whereas the damping ratio gradually increased, indicating that the two models had been damaged under the earthquake and that the degree of damage increased with an increase in the earthquake acceleration. In comparison, the first two frequencies of the normative model were reduced by 37.7% and 17.4% at the end of case 22; similarly, the first two frequencies of the optimization model were reduced by 32.7% and 16.7%, showing that the natural vibration frequency of the normative model decreased faster than that of the optimization model. Under the action of an earthquake, structural damage will lead to a decrease in the natural vibration frequency. Many previous studies have shown that the level of damage becomes more serious with faster decreases in the natural frequency under the action of an earthquake [24, 25]. Therefore, the normative model was damaged more severely

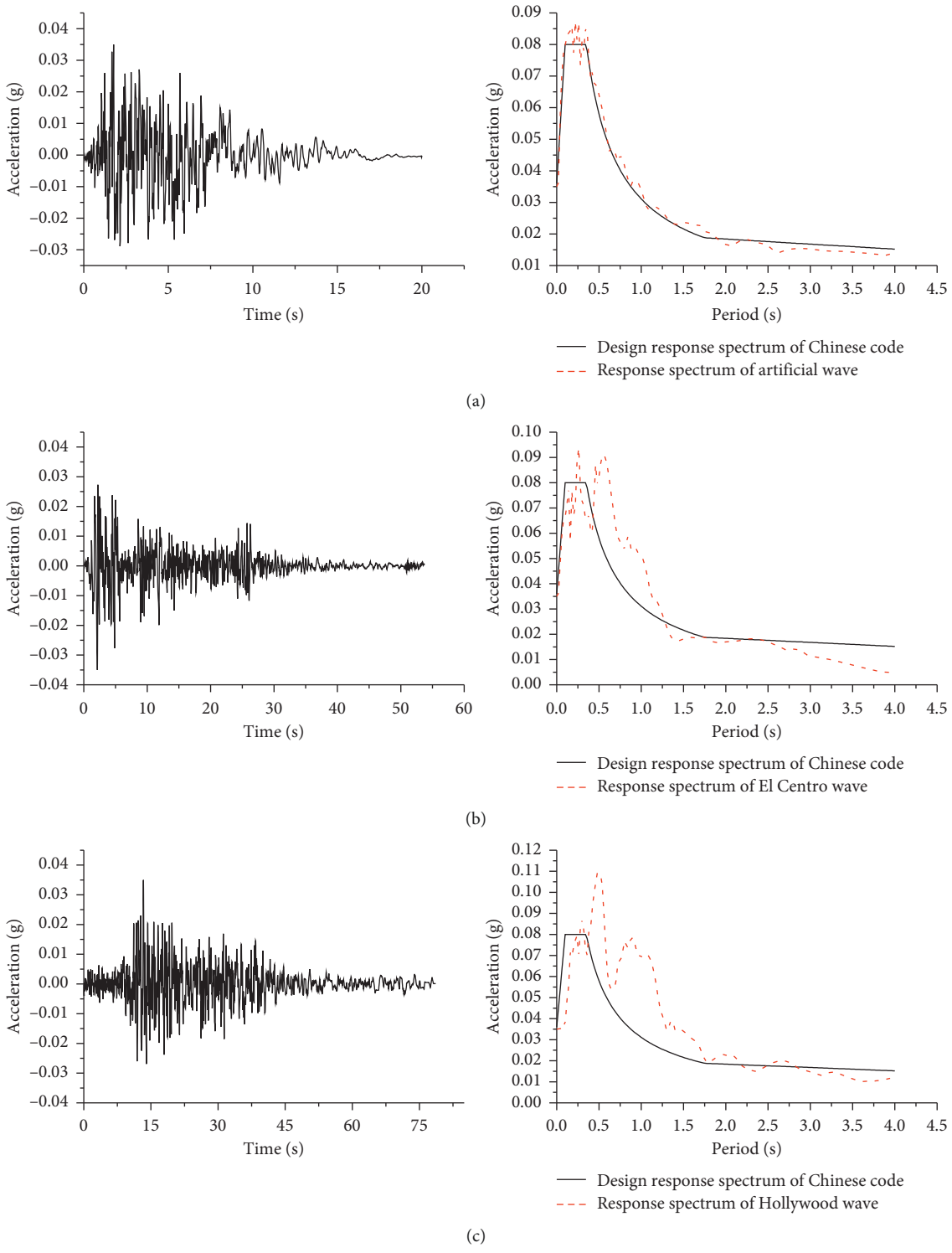

Figure 4: Time-history curve and response spectrum of the input ground motion. (a) Artificial wave, (b) El Centro, and (c) Hollywood.

Table 9: Peak accelerations of different level of intensity (cm/s^2).

Fortification intensity	Intensity 7	Intensity 7 (0.15 g)	Intensity 8
Frequent	35	55	70
Basic	100	150	200
Rare	220	310	400

Table 10: Test procedure.

Test cases	Case designation	Intensity	Input excitation	Peak value of input acceleration (g)
1	W1	White noise		0.105
2	F7R		RH1TG035	0.105
3	F7E	Frequent 7	El Centro	0.105
4	F7H		Hollywood	0.105
5	W2	White noise		0.105
6	F8R		RH1TG035	0.21
7	F8E	Frequent 8	El Centro	0.21
8	F8H		Hollywood	0.21
9	W3	White noise		0.105
10	B7R		RH1TG035	0.3
11	B7E	Basic 7	El Centro	0.3
12	B7H		Hollywood	0.3
13	W4	White noise		0.105
14	B7.5R		RH1TG035	0.45
15	B7.5E	Basic 7 (0.15 g)	El Centro	0.45
16	B7.5H		Hollywood	0.45
17	W5	White noise		0.105
18	R7R		RH1TG035	0.66
19	R7E	Rare 7	El Centro	0.66
20	R7H		Hollywood	0.66
21	W6	White noise		0.105
22	H0.76	0.76 g	Hollywood	0.76
23	W7	White noise		0.105

than the optimization model under the action of a strong earthquake according to the relationship between the damage and the natural frequency. In addition, the damping ratio in the optimization model became larger than that in the normative model under the action of a strong earthquake, which means that the optimization model has a stronger energy dissipation potential.

4.3. Damage Analysis for Components. The damage suffered by an actual structure is generally described by the characteristics of cracks on the surfaces of the components of that structure. However, such cracks can be described only by limited qualitative descriptions; that is, they cannot be effectively described quantitatively. In response to this problem, some influencing factors should be chosen to analyze the component damage states. The component-based Park-Ang damage model [26] and the material-based damage model [27] show that the deformation and strain of a component have a direct correlation with the damage suffered by the component. Excessive deformation of a component will lead to excessive strain, which inevitably leads to the cracking of concrete or the crushing of a component; in other words, the larger the deformation or strain of a component, the more severe the component damage. In view of this relationship, the strain of a component can be chosen to quantitatively compare the seismic damage performances of the two models in the tests. Because the damage done to a structure cumulatively increases under an earthquake and does not disappear with variations in the seismic wave, it is more meaningful to compare the cumulative damage suffered under the three seismic waves under the same earthquake intensity. Therefore, the envelope of the maximum strain value under each seismic wave was selected for an analysis of the damage suffered by the components.

4.3.1. Horizontal Component. The strains of the horizontal components such as the coupling beam and frame beam were extracted for a comparison of their damage states, as shown in Figures 6 and 7. A comparison shows that the strain distributions of the horizontal components in both of the models were similar under the same earthquake activity, and the maximum strain appeared on the middle floors of both models. In the case of a frequent earthquake with an intensity of 7, the distributions of the strain values in both models were approximately identical along the structural height, as shown in Figures 6(a) and 7(a). However, with an increase in the earthquake acceleration, the strain values in the two models became different. As shown in Figures 6(b) and 7(b), the strains of the coupling beams and the frame beams in the optimization model were obviously larger than those in the normative model under the basic earthquake with an intensity of 7, and the difference in the strain between the two models became increasingly obvious under the rare earthquake with an intensity of 7, as shown in Figures 6(c) and 7(c). To analyze the strain evolution throughout the entire experiment, the strains of the horizontal components on the 8th and 11th floors were extracted, as shown in Figure 8. In comparison, the strain in the optimization model increased more rapidly than that in the normative model throughout the entire test except for the cases involving frequent earthquakes with intensities of 7 and 8. Through detailed observations acquired after the test was complete, the bearing capacities of the horizontal components remained stable. These findings indicate that

(a) (b) (c) (d)

Figure 5: Crack of typical components: (a) coupling beam, (b) frame beam, (c) slab of beam end, and (d) intersection of column and beam.

Table 11: Damping and frequency of normative model.

PGA (g)	0.105	0.21	0.3	0.45	0.66	0.76
Primary frequency	3.13	3.13	2.95	2.73	2.34	1.95
Second mode frequency	10.16	9.77	9.77	9.38	8.78	8.39
Damping ratio (%)	5.7	5.7	5.81	6.42	7.35	7.54

Table 12: Damping and frequency of optimization model.

PGA (g)	0.105	0.21	0.3	0.45	0.66	0.76
Primary frequency	3.03	3.03	2.73	2.54	2.34	2.04
Second mode frequency	9.77	9.38	8.98	8.78	8.39	8.14
Damping ratio (%)	5.51	5.51	5.82	6.65	7.6	7.75

the horizontal components in the optimization model suffered greater damage and that the damage suffered by those components increased more rapidly during the strong earthquake than did those in the normative model, which is in accordance with the aim of damage optimization.

4.3.2. Vertical Component. No observations revealed obvious visible cracks on the surfaces of the vertical components. The strains of the vertical components of the two models were compared and analyzed to further investigate the damage suffered by the vertical components. Figures 9 and

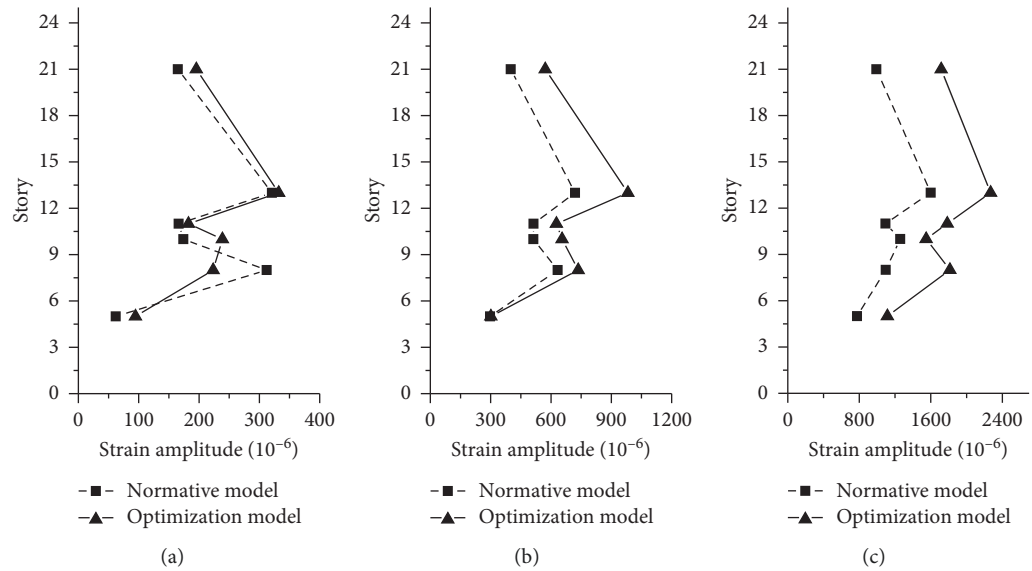

Figure 6: Maximum strain value of coupling beam at different story. (a) Frequent intensity 7, (b) basic intensity 7, and (c) rare intensity 7.

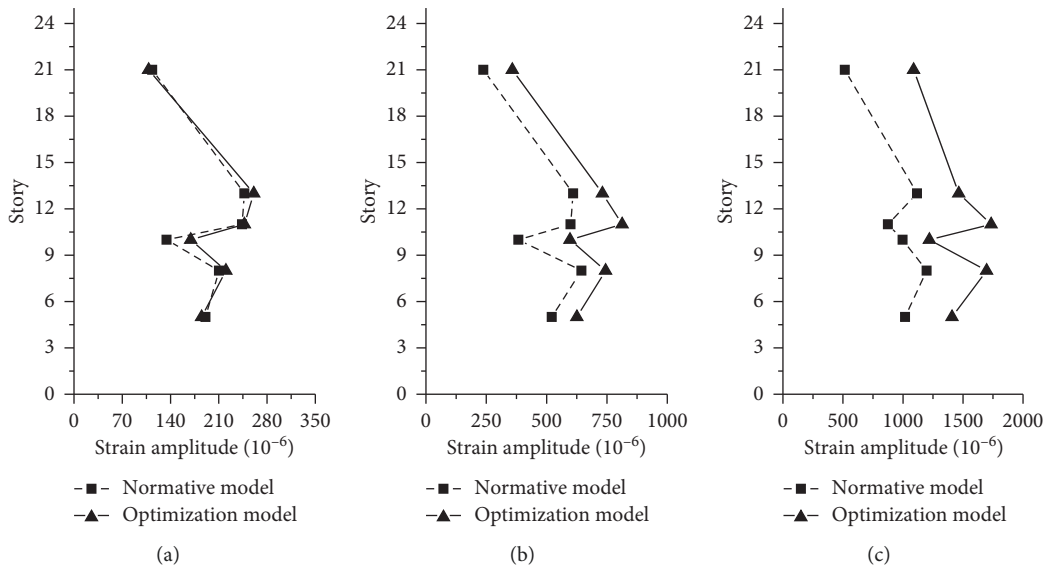

Figure 7: Maximum strain value of frame beam at different story. (a) Frequent intensity 7, (b) basic intensity 7, and (c) rare intensity 7.

10 show that the strain distributions in both models were similar under the same earthquake activity, and the strain values on the ground floor were much larger than those on the upper floors. However, the strain values in the two models developed different characteristics with an increase in the earthquake acceleration. In the case of frequent earthquakes with an intensity of 7, the strain values of the vertical components in both models were approximately identical along the structural height. However, in the cases of both basic and rare earthquakes with an intensity of 7, the strain values in the normative model became larger than those in the optimization model on the same floors. Through a further comparison of the damage suffered by the frame columns in the two models, comparatively large strains were found on the middle floors of the normative model (but not the ground floor) under the action of a strong earthquake, as shown in Figure 10(c), whereas the strains in the optimization model were reasonably limited. This result indicates that abrupt changes in the damage state may have occurred in the frame columns on the middle floors of the normative model. To analyze the strain evolution throughout the entire experiment, the strains of the vertical component on the 1st and 11th floors were extracted, as shown in Figure 11. The strains in the normative model were obviously larger than those in the optimization model during the entire test except for the cases involving frequent earthquakes. This finding means that the development of damage in the vertical components in the optimization model can be limited under

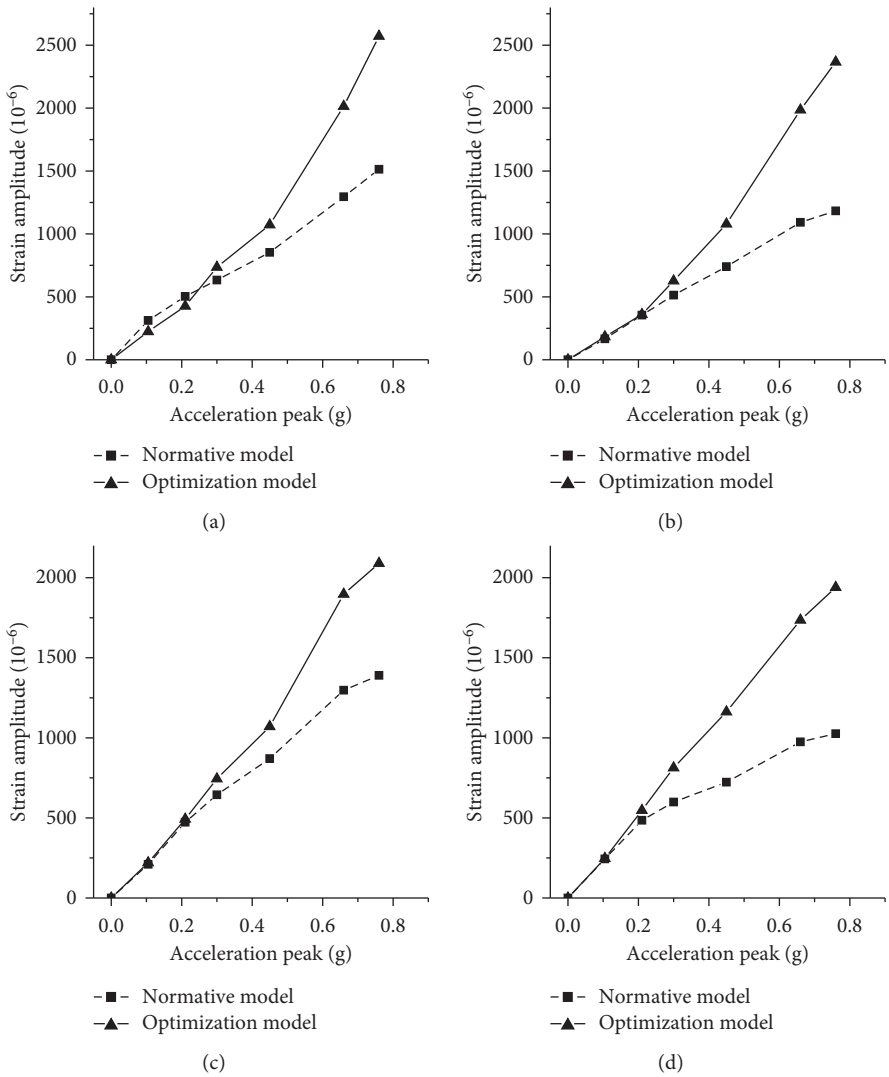

Figure 8: Damage evolution of horizontal component. (a) Coupling beam at 8 story, (b) coupling beam at 11 story, (c) frame beam at 8 story, and (d) frame beam at 11 story.

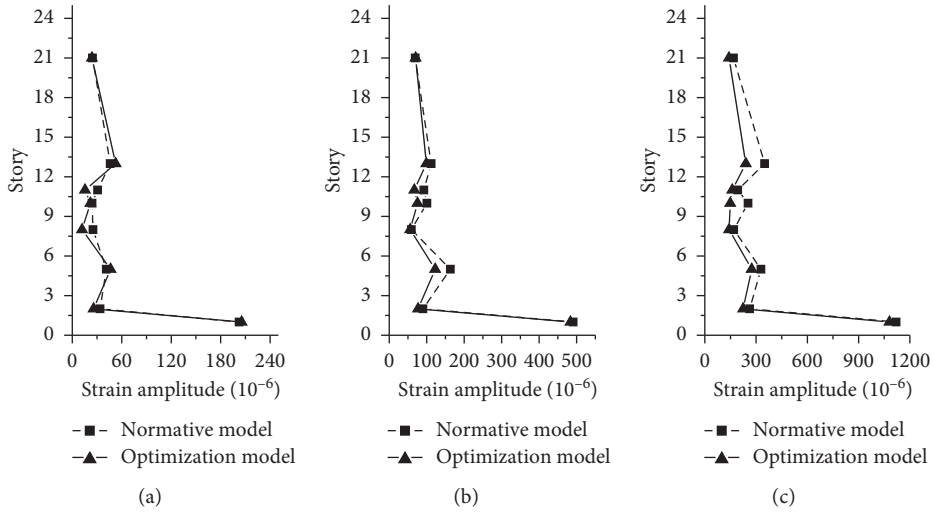

Figure 9: Maximum strain value of wall limb at different story. (a) Frequent intensity 7, (b) basic intensity 7, and (c) rare intensity 7.

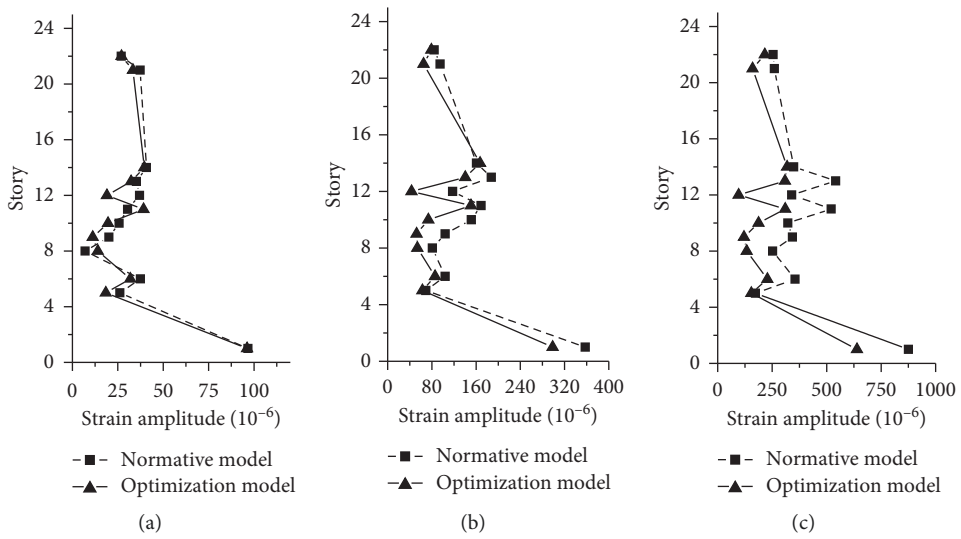

Figure 10: Maximum strain value of frame column at different story. (a) Frequent intensity 7, (b) basic intensity 7, and (c) rare intensity 7.

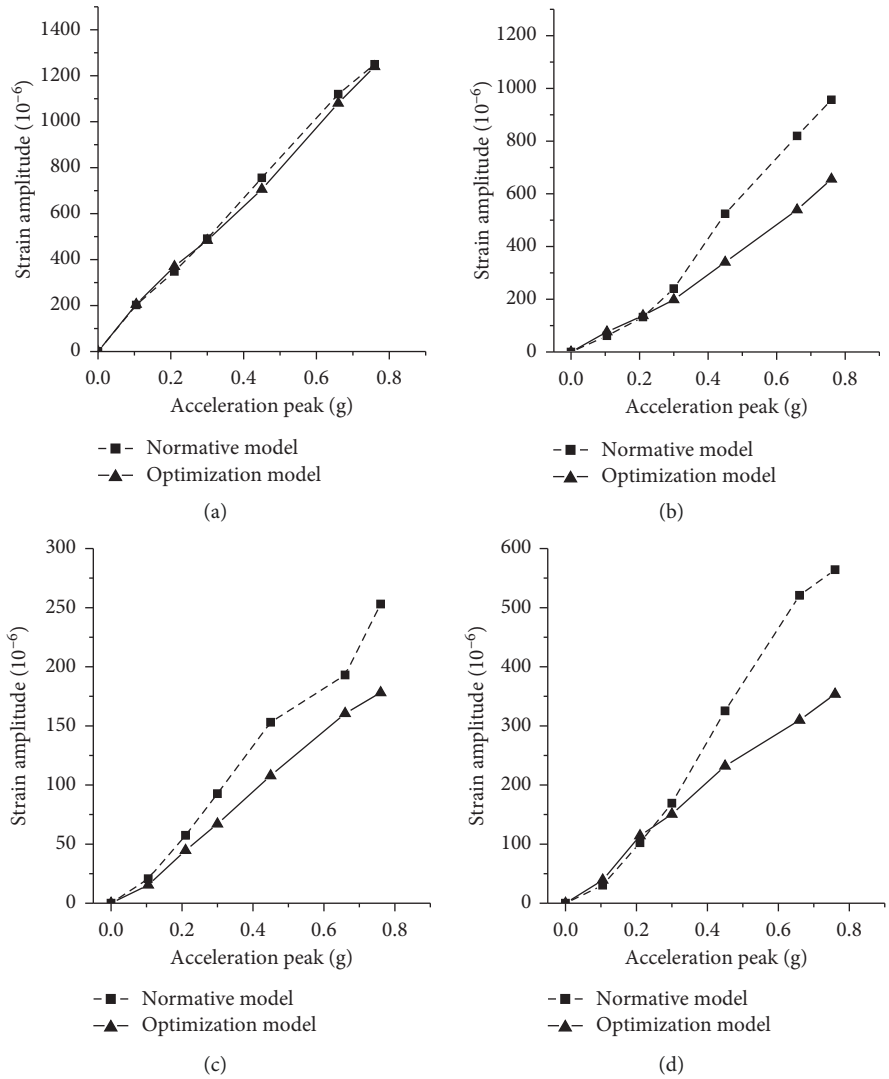

Figure 11: Damage evolution of vertical component. (a) Wall limb at 1 story, (b) frame column at 1 story, (c) wall limb at 11 story, and (d) frame column at 11 story.

strong earthquakes and that the bearing capacity of those vertical components may remain more stable during a strong earthquake.

4.3.3. Relationship between Damages in Horizontal Component and Vertical Component. According to the comparative analysis of the component damage states in the previous section, the increase in the damage sustained by the horizontal components and the decrease in the damage sustained by the vertical components in the optimization model change the relationship among the damage states in both kinds of components. As shown in Figure 12, the values of $\varepsilon_L/\varepsilon_c$ and $\varepsilon_{LL}/\varepsilon_w$ can reflect the relationship among the damage states in the horizontal and vertical components, where ε_L, ε_{LL}, ε_c, and ε_w represent the maximum strain values for the frame beam, coupling beam, frame column, and wall limb, respectively, on each floor. The values of $\varepsilon_L/\varepsilon_c$ and $\varepsilon_{LL}/\varepsilon_w$ in the two model structures are both greater than 1, indicating that the damage suffered by the horizontal components is greater than that by the vertical components, which suggests that the two seismic damage mechanisms, namely, "strong wall limb-weak coupling beam" and "strong frame column-weak frame beam," are both realized on each floor. However, the values of $\varepsilon_L/\varepsilon_c$ and $\varepsilon_{LL}/\varepsilon_w$ in the optimization model are apparently greater than those in the normative model on each floor, indicating that regions with greater damage were concentrated on the horizontal components and that the damage to the vertical component was relatively reduced in the optimization model in comparison with the normative model.

In the seismic design for a frame-core tube structure, the abovementioned relationship among the damage states in the vertical and horizontal components on the same floor is able to prevent only the development of soft-story behaviors, that is, this relationship does not ensure the development of a global damage mechanism [28–31]. This kind of damage mechanism can be described by the relationship among the damage states in the vertical components on the ground floor and the horizontal components on the upper floors; in this case, the damage suffered by the vertical components should be reasonably limited to ensure that its damage is smaller than that suffered by the horizontal components on the upper floors. As shown in Figures 13 and 14, under a rare earthquake, the damage sustained by the horizontal components on the upper floors in the normative model is close to that sustained by the vertical components on the ground floor. However, this kind of relationship among component damage states cannot ensure that the energy dissipation capacity and ductility of the horizontal components are maximized [13]. In contrast, the damage sustained by the horizontal components on each floor in the optimization model were apparently greater than those sustained by the vertical components on the ground floor; consequently, a global damage mechanism developed easily under earthquake activity. In other words, the "strong wall limb-weak coupling beam" and "strong frame column-weak frame beam" damage mechanisms in the optimization model can be applied more effectively to the entire structure than to the individual floors of the structure.

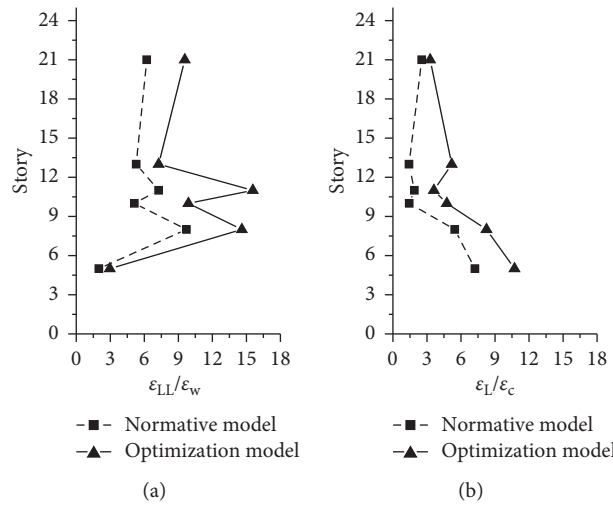

Figure 12: Strain ratio between vertical component and horizontal component. (a) Strain ratio of coupling beam and wall limb; (b) strain ratio of frame beam and frame column.

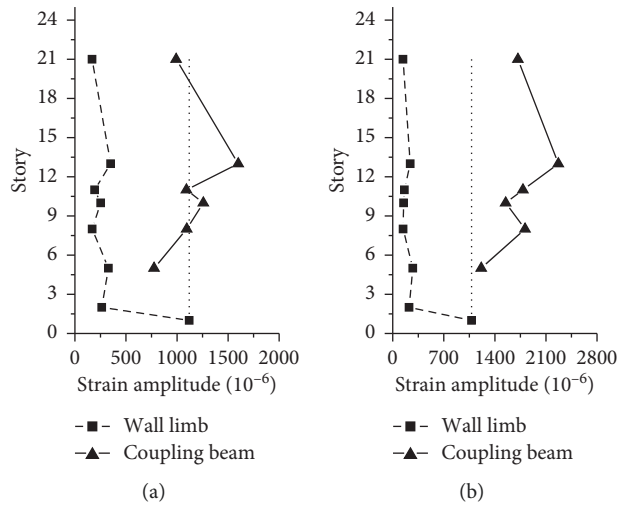

Figure 13: Comparison of strains in coupling beam and wall limb under rare earthquake. (a) Normative model; (b) optimization model.

4.3.4. Relationship between Damages in the Wall Limb and Frame Column. Due to the differences in the damage sustained by the vertical components in the two models under the action of a strong earthquake, the relationship among the damage states of these components may influence the collaborative working mechanism between the outer frame and core tube. The value of $\varepsilon_c/\varepsilon_w$ can reflect the relationship among the damage states of the frame column and wall limb, where ε_c and ε_w represent the maximum strain values for the frame column and wall limb, respectively, on each floor. According to the distributions of damage within the frame columns and shear walls, the damage on the ground floor is generally the largest, and thus, the damage sustained at the ground floor plays a substantial role in controlling the abovementioned collaborative working mechanism. The $\varepsilon_c/\varepsilon_w$ values on the ground floors of the two models were extracted,

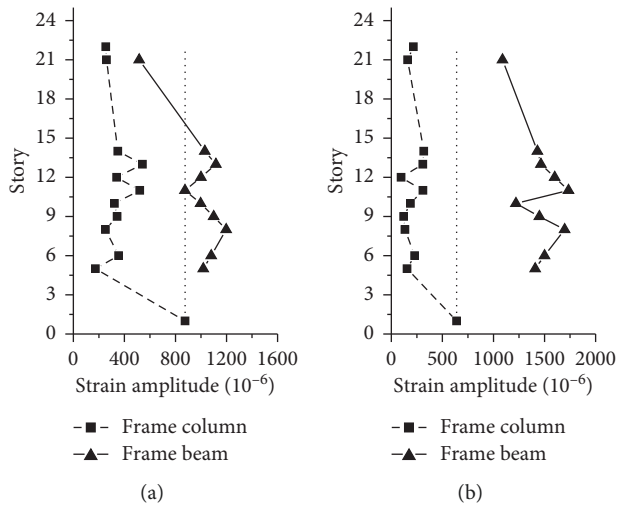

Figure 14: Comparison of strains in frame beam and frame column under rare earthquake. (a) Normative model; (b) optimization model.

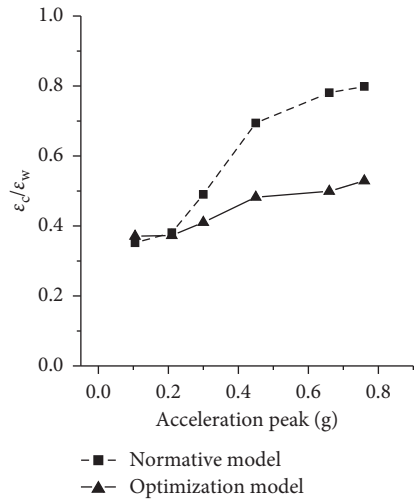

Figure 15: Strain ratio of column and wall limb.

as shown in Figure 15. The values of $\varepsilon_c/\varepsilon_w$ in the two models are both less than 1, indicating that the damage sustained by the frame column is less severe than that sustained by the wall limb; hence, the collaborative working mechanism is realized in both models. Through further comparison, the values of $\varepsilon_c/\varepsilon_w$ in the normative model clearly increased more than those in the optimization model with an increase in the acceleration peak. This finding indicates that the frame column on the ground floor in the normative model was damaged more severely with an increase in the earthquake level, and thus, the reliability of the bearing capacity of the outer frame serving as the second line of fortification cannot be ensured. In contrast, the damage sustained by the frame column on the ground floor was limited more effectively in the optimization model, with which an antiseismic design fortification line can be better implemented and the collaborative working mechanism can be better realized.

4.4. Overall Damage Analysis. The increase in the damage sustained by the horizontal components and the decrease in the damage sustained by the vertical components throughout the structure inevitably influence the overall structural damage. In this paper, to comprehensively consider the adverse effects of structural stiffness degradation and second-order gravity effects on high-rise buildings, an evaluation index based on the degradation of the equivalent rigidity-to-weight ratio is used to represent the overall damage [32] and is expressed as follows:

$$F = 1 - \frac{\lambda_i^2}{\lambda_0^2}, \tag{4}$$

where F is the structure failure index, λ_0 is the initial ratio of equivalent rigid-to-weight, and λ_i is the instantaneous ratio of equivalent rigidity-to-weight after suffering structural damage. The formula for λ_i is [32].

$$\lambda_i = \frac{K_{\text{eqi}}}{GH^2}, \tag{5}$$

where K_{eqi} is the equivalent lateral stiffness at any moment of stiffness degradation, G is the weight of the structure, and H is the total height of the structure. The two model structures have the same value of G and H. Therefore λ_i is determined by K_{eqi}. Due to the different damage performance of the two model structure, the variations in equivalent lateral stiffness are inevitably affected during the tests. According to the literature [32], the equivalent stiffness K_{eqi} is a parameter which is used to represent the overall stiffness of structure under the action of an earthquake. Thus, in this paper, the stiffness of equivalent single-degree-of-freedom system (SDOF) can be used to represent K_{eqi}. To calculate K_{eqi}, the model structure was transformed into the SDOF system using the shape vector based on the first modal shape of the structure. The equation for the equivalent SDOF system is given as follows: [33].

$$M\ddot{x} + C\dot{x} + Kx = -M\ddot{x}_g, \tag{6}$$

where M, C, and K denote the properties of the equivalent SDOF system. Therefore K_{eqi} can be expressed by K as follows:

$$K_{\text{eqi}} = K = M * (2\pi f)^2, \tag{7}$$

where f_i is the primary natural frequency of the structure after the ith earthquake.

Equations (5) and (7) are presented in equation (4) to obtain the variation in the overall damage index at different earthquake levels, as shown in Table 13.

The relationship between the damage grade and the range of the index is shown in Table 14 [32]. Figure 16 shows the curves of the overall damage sustained by both models at different earthquake levels. The overall damage indices of both models are 0 under frequent earthquakes with intensities of 7 and 8 in accordance with experimental phenomena. With an increase in the acceleration, the overall damage suffered within the optimization model under basic earthquake activities was larger than that within the normative model because the horizontal components became

Table 13: Overall damage index value at different earthquake levels.

PGA (g)	0.105	0.21	0.3	0.45	0.66	0.76
Normative model	0	0	0.11	0.24	0.44	0.61
Optimization model	0	0	0.1	0.29	0.41	0.54

Table 14: Damage index range at different damage levels.

Damage level	Basic integrity	Slight damage	Moderate damage	Serious damage	Collapse
F	≤0.1	0.1~0.2	0.2~0.5	0.5~0.75	≥0.75

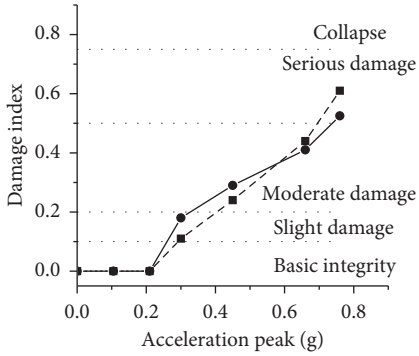

Figure 16: Overall damage.

damaged in the optimization model faster than those in the normative model due to the damage optimization, which led to faster degradation in the early stage of the overall stiffness deterioration of the structure. With a further increase in the acceleration, the overall damage suffered within the optimization model became smaller than that within the normative model under the action of a strong earthquake, showing that the overall stiffness deterioration of the optimization model was effectively controlled during the strong earthquake because the damage sustained by the vertical components, especially the frame column in the outer frame, was effectively limited under such conditions.

4.5. Shear Force and Overturning Moment. Due to the increase in the damage sustained by the horizontal components and the decrease in the damage sustained by the vertical components, the structures consequently exhibited different internal force responses. The maximum story shears of the two models are shown in Figures 17 and 18. Under the activities of frequent earthquakes with an intensity of 7, the story shears in both models gradually increased from the upper floor to the lower floor, thereby showing an obvious triangular distribution along the structural height. The distributions were similar under the three different seismic waves because the two models still behaved elastically under frequent earthquakes. With an increase in the acceleration peak, the distribution of the story shear in the normative model changed obviously under the activities of strong earthquakes, whereas that in the optimization model varied little, as shown in Figures 17(b) and 18(b). These results indicate that the internal force response of the optimization model under the activities of strong

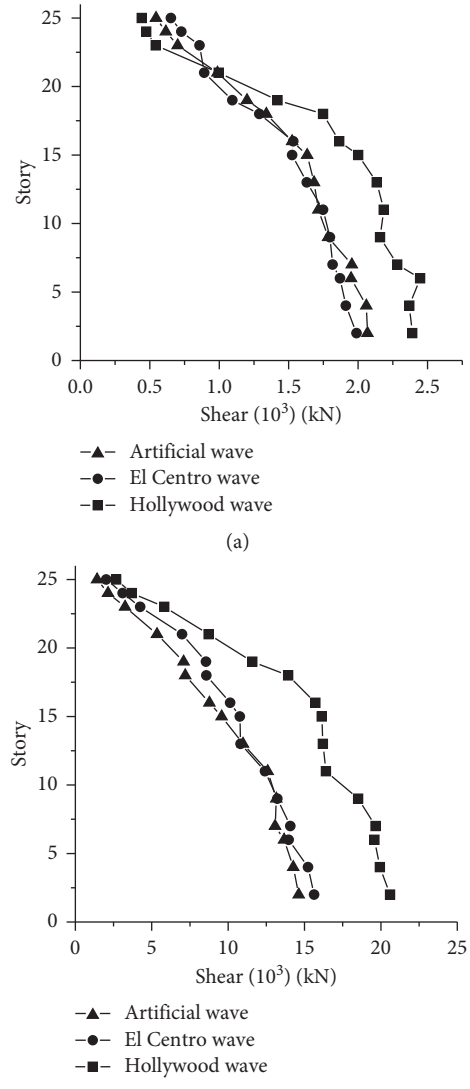

Figure 17: Story maximum shear of optimization model. (a) Frequent intensity 7; (b) rare intensity 7.

earthquakes was more stable than that of the normative model, making it easier to actively control the seismic capability of the structure in the seismic design. By further comparing the story shear with the overturning moment on each floor, the story shear and the overturning moment of the optimization model under the action of a rare earthquake were both smaller than those in the normative model,

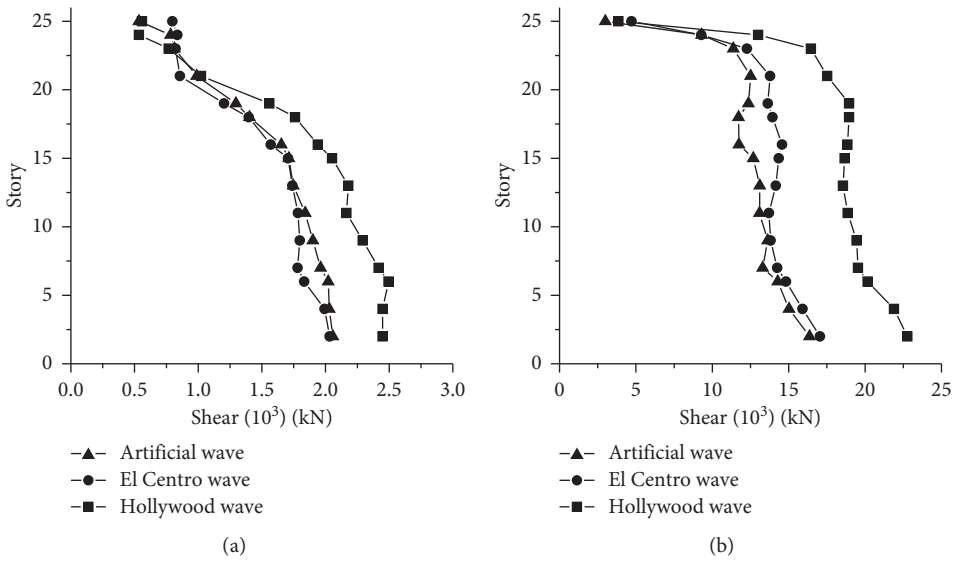

Figure 18: Story maximum shear of normative model. (a) Frequent intensity 7; (b) rare intensity 7.

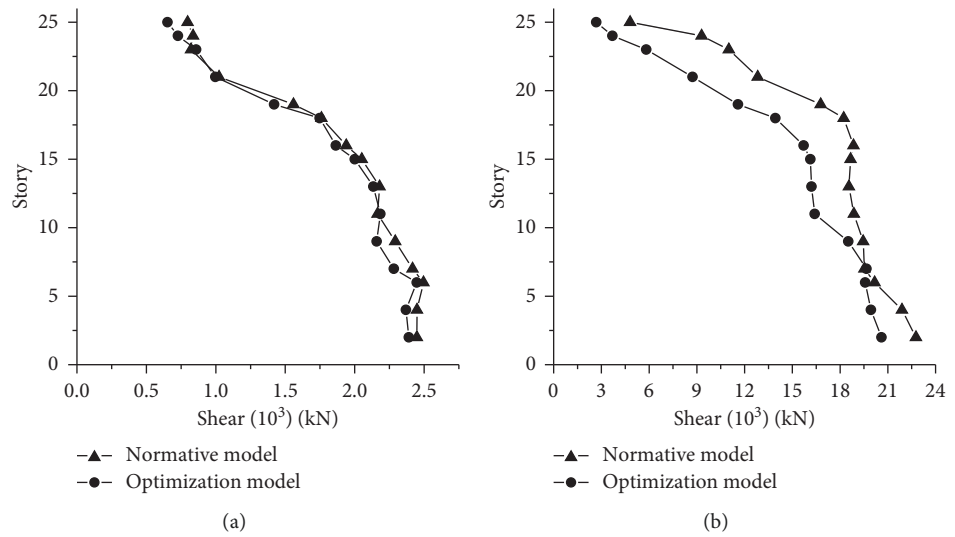

Figure 19: Comparison of story maximum shear. (a) Frequent intensity 7; (b) rare intensity 7.

as shown in Figures 19 and 20. The relationship among the component damage states in the optimization model could further reduce the seismic demand of the internal force, thereby making the structure more resistant to earthquakes.

5. Conclusions

In this paper, the component damage states in two models were experimentally and analytically investigated. The following conclusions can be drawn from the shaking table tests performed herein:

(1) In comparison with the variations in the frequencies and damping ratios of the two models, the optimization model was damaged less severely and had a stronger energy dissipation potential than the normative model under the action of a strong earthquake.

(2) The horizontal components, whose damage was optimized in the optimization model, can undergo greater damage; thus, the ductility in the nonlinear damage stage and the postyield bearing capacity can be exploited during an earthquake. The constraint on the damage sustained by the vertical components in the optimization model can permit the bearing capacity to remain more stable during a strong earthquake.

(3) The optimization of the relationship among the damage states of the horizontal and vertical components in the optimization model causes the regions exhibiting greater damage to become concentrated on the horizontal components. Moreover, a global damage mechanism can be developed during a strong earthquake, and thus, the energy dissipation

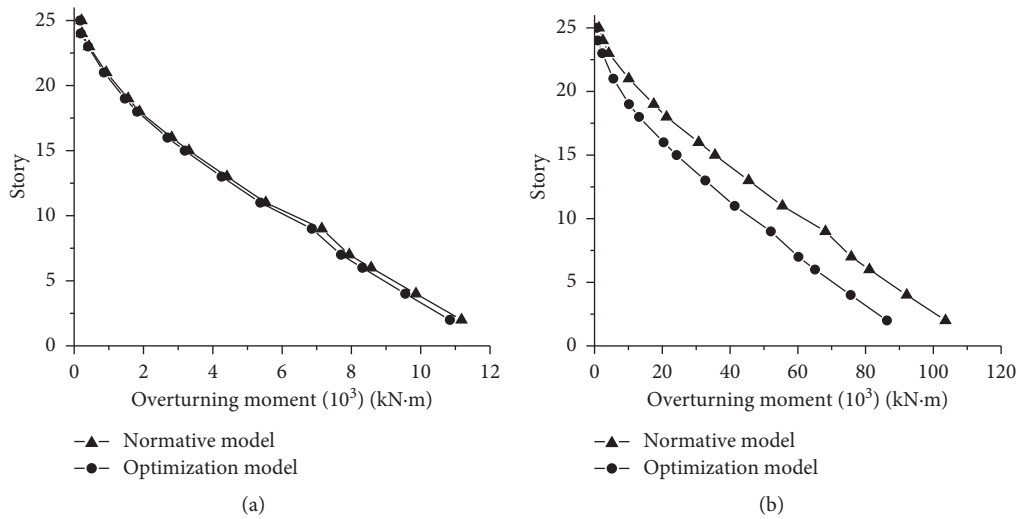

Figure 20: Comparison of maximum overturning moment. (a) Frequent intensity 7; (b) rare intensity 7.

capacity and ductility of the horizontal components can be more effectively maximized. In addition, the optimization of the damage sustained by the vertical components can ensure the reliability of the bearing capacity of the outer frame acting as a second fortification line, further optimizing the relationship among the damage states of the frame columns and wall limbs and better implementing the collaborative working mechanism between the two lateral force systems in the frame-core tube structure.

(4) The results of an overall damage evaluation prove that an increase in the damage sustained by the horizontal components and a decrease in the damage sustained by the vertical components in the optimization model can effectively limit the overall stiffness deterioration and the development of overall damage during strong earthquakes in comparison with the normative model.

(5) The internal force response can be further optimized due to the increase in the damage sustained by the horizontal components and the decrease in the damage sustained by the vertical components in the optimization model. The distribution of the story shear along the height of the structure can be improved during a strong earthquake, and the demand on the bearing capacity of the structure can be further reduced, making the structure more resistant to earthquakes.

Data Availability

All data supporting the findings of this study are available upon request from the corresponding author.

Conflicts of Interest

The authors declare that they have no conflicts of interest.

Acknowledgments

This research is supported by the National Key Research and Development Program of China under grant no. 2016YFC0701102, the Major Program of National Natural Science Foundation of China under grant no. 51538003, China Major Development Project for Scientific Research Instrument under grant no. 51827811, Shenzhen Technology Innovation Program under grant no. JCYJ20170811160003571 and the Research Project of Knowledge Innovation Plan in Shenzhen (JCYJ20160531193340540).

References

[1] G. Ma, H. Hao, and Y. Zhou, "Assessment of structure damage to blasting induced ground motions," *Engineering Structures*, vol. 22, no. 10, pp. 1378–1389, 2000.

[2] M. Sanchez-Silva and L. Garcia, "Earthquake damage assessment based on fuzzy logic and neural networks," *Earthquake Spectra*, vol. 17, no. 1, pp. 89–112, 2001.

[3] P. Khashaee, "Damage-based seismic design of structures," *Earthquake Spectra*, vol. 21, no. 2, 2005.

[4] J. Ou, H. Zheng, B. Wu et al., "Seismic damage performance-based design of reinforced concrete structures," *Earthquake Engineering & Engineering Vibration*, vol. 2, no. 3, pp. 173–184, 1999.

[5] D. Jian, "Research on seismic capacity design method of RC frame based on direct damage," *World Earthquake Engineering*, vol. 23, no. 4, pp. 199–204, 2007.

[6] J. Xia, W. Yang, W. Zhang et al., "Direct damage-based seismic design method for RC frame structures," *Building Structure*, vol. 42, pp. 210–214, 2012.

[7] G. S. Kamaris, G. D. Hatzigeorgiou, and D. E. Beskos, "Direct damage controlled seismic design of plane steel degrading frames," *Bulletin of Earthquake Engineering*, vol. 13, no. 2, pp. 587–612, 2015.

[8] Z. Tian, X. Zhang, and T. Zhao, "Seismic damage of multilayer reinforced concrete frame structures in Wenchuan earthquake," *Building Structure*, vol. 39, no. 11, pp. 67–71, 2009.

[9] Z. W. Miao, Z. Y. Qiu, and Y. Ming, "Study on energy dissipation mechanism and collapse-resistant performance of RC frame-shear-wall structure under strong earthquake," *Applied Mechanics and Materials*, vol. 204–208, pp. 2550–2554, 2012.

[10] H. D. Yun, P. Wanshin, L. Joohwa et al., "Behavior characteristics of coupled shear wall on effects of coupling beam details," *Journal of the Architectural Institute of Korea Structure & Construction*, vol. 20, no. 6, pp. 19–26, 2004.

[11] Q. U. Zhe and Y. E. Lieping, "Seismic design methodology based on damage mechanism control for reinforced concrete structures," *Journal of Building Structures*, vol. 32, no. 10, pp. 21–29, 2011.

[12] G. M. Verderame, F. De Luca, P. Ricci, and G. Manfredi, "Preliminary analysis of a soft-storey mechanism after the 2009 L'Aquila earthquake," *Earthquake Engineering & Structural Dynamics*, vol. 40, no. 8, pp. 925–944, 2011.

[13] R. Montuori and R. Muscati, "A general design procedure for failure mechanism control of reinforced concrete frames," *Engineering Structures*, vol. 118, pp. 137–155, 2016.

[14] Z. Miao, "Distribution mode of hysteretic energy and damage mechanism of RC frame-shear-wall structure under strong earthquakes," *Journal of Southeast University*, vol. 42, no. 5, pp. 933–939, 2012.

[15] J. Zhang, Y. Wu, C. Yang et al., "Study on seismic performance of super high-rise frame-core tube structures under long-period ground motions," *Building Structure*, vol. 44, no. 19, pp. 40–45, 2014.

[16] X. Lu, M. Li, H. Guan, X. Lu, and L. Ye, "A comparative case study on seismic design of tall RC frame-core-tube structures in China and USA," *Structural Design of Tall and Special Buildings*, vol. 24, no. 9, pp. 687–702, 2015.

[17] X. Lu, B. Zhou, B. Zhao et al., "Shaking table test and numerical analysis of a high-rise building with steel reinforce concrete column and reinforce concrete core tube," *Structural Design of Tall & Special Buildings*, vol. 24, no. 18, pp. 1019–1037, 2016.

[18] Ministry of Housing and Urban–Rural Development of the People's Republic of China, *Technical Specification for Concrete Structures of Tall Buildings JGJ3-2010*, Architecture & Building Press, Beijing, China, 2010, English version.

[19] Ministry of Housing and Urban–Rural Development of the People's Republic of China, *Code for Seismic Design of Buildings GB 50011-2010*, Architecture & Building Press, Beijing, China, 2010, English version.

[20] Ministry of Housing and Urban–Rural Development of the People's Republic of China, *Code for Design of Concrete Structure GB 50011-2010*, Architecture & Building Press, Beijing, China, 2010, English version.

[21] M. Bosco and L. Tirca, "Numerical simulation of steel I-shaped beams using a fiber-based damage accumulation model," *Journal of Constructional Steel Research*, vol. 133, pp. 241–255, 2017.

[22] C. He, Q. Cao, J. Teng et al., "Research on the damage distribution patterns of frame-core tube structure based on material damage of components," *Building Structure*, vol. 41, pp. 1003–1006, 2011.

[23] M. Poursha and M. A. Amini, "A single-run multi-mode pushover analysis to account for the effect of higher modes in estimating the seismic demands of tall buildings," *Bulletin of Earthquake Engineering*, vol. 13, no. 8, pp. 2347–2365, 2015.

[24] A. S. Cakmak and S. Rodriquezgomez, "Evaluation of seismic damage indices for reinforced concrete structures," *Applied Artificial Intelligence*, vol. 19, no. 9-10, pp. 861–879, 1990.

[25] J.-F. Wang, C.-C. Lin, and S.-M. Yen, "A story damage index of seismically-excited buildings based on modal frequency and mode shape," *Engineering Structures*, vol. 29, no. 9, pp. 2143–2157, 2007.

[26] Y. J. Park and A. H. S. Ang, "Mechanistic seismic damage model for reinforced concrete," *Journal of Structural Engineering*, vol. 111, no. 4, pp. 722–739, 1985.

[27] M. R. Salari, S. Saeb, K. J. Willam, S. J. Patchet, and R. C. Carrasco, "A coupled elastoplastic damage model for geomaterials," *Computer Methods in Applied Mechanics and Engineering*, vol. 193, no. 27–29, pp. 2625–2643, 2004.

[28] A. Heidari and S. Gharehbaghi, "Seismic performance improvement of special truss moment frames using damage and energy concepts," *Earthquake Engineering & Structural Dynamics*, vol. 44, no. 7, pp. 1055–1073, 2015.

[29] E. A. Godínez-Domínguez and A. Tena-Colunga, "Nonlinear behavior of code-designed reinforced concrete concentric braced frames under lateral loading," *Engineering Structures*, vol. 32, no. 4, pp. 944–963, 2010.

[30] J. Bai and J. Ou, "Realization of the global yield mechanism of RC frame structures by redesigning the columns using column tree method," *Science China Technological Sciences*, vol. 58, no. 10, pp. 1627–1637, 2015.

[31] B. I. Stojadinovic, S. C. Goel, and S. Leelataviwat, "Energy-based seismic design of structures using yield mechanism and target drift," *Journal of Structural Engineering*, vol. 128, no. 8, pp. 1046–1054, 2002.

[32] L. Hai-Xia, J. Teng, L. I. Zuo-Hua et al., "Failure discrimination for high-rise diagrid tube structures based on overall stability," *Journal of Vibration & Shock*, vol. 32, no. 24, pp. 96–103, 2013.

[33] H. Krawinkler and G. D. P. K. Seneviratna, "Pros and cons of a pushover analysis of seismic performance evaluation," *Engineering Structures*, vol. 20, no. 4–6, pp. 452–464, 1998.